Interlocked hybrid-cell Kirigami inspired cellular structures and their vibroacoustic performance

Simone Broccolo, Morvan Ouisse, Emmanuel Foltete, Fabrizio Scarpa

Interlocked hybrid-cell Kirigami inspired cellular structures and their vibroacoustic performance

S. Del Broccolo[1], M. Ouisse[1], E. Foltete[1], F. Scarpa[2]
[1] Univ. Bourgogne Franche-Comté, FEMTO-ST Institute, CNRS/UFC/ENSMM/UTBM
Department of Applied Mechanics, 25000 BESANÇON-FR
e-mail: **simone.del.broccolo@gmail.com**

[2] Bristol Composites Institute (ACCIS), University of Bristol
Queen's Building, University Walk, Bristol BS8 1TR, United Kingdom

Abstract
Sandwich panels are widely used in applications where high stiffness and low weight structures have become an asset, such as the aerospace segment. The environment in which those panels are used produce uncomfortable vibrations in the low-mid range which also may induce inefficiency. This hybrid cellular core obtained with a Kirigami derived technique and intended to be used for sandwich panels, is investigated, parametrically, by performing numerical simulations and varying the topology. The vibration filtering characteristic of this innovative cellular core is compared to more classic configurations. The comparison is carried out using the Wave Finite Element Method (WFEM) by analysing only the unit cell thanks to the Floquet-Bloch theorem periodic conditions. Harmonic numerical simulations using commercial FEA software are also carried out to illustrate the validity of the bandgaps location and width. We will base the vibration performance evaluation analysing in-plane and out-of-plane bandgaps.

1 Introduction

Many efforts have been produced so far to better understand the dynamic behaviour of complex periodic structures. This is a direct consequence of the increase of such structures in the engineering domain. Some examples like train rails, bridges and skyscrapers can be encountered in everyday life but we can also find them in the Aerospace engineering field, where stiffened plates as well as composites sandwich panels are widely used. Those type of structures become convenient in terms of manufacturing as it is easier to produce a single item that can be used to create different final shapes rather than having to customize the manufacturing process to each application. The solicitations that an airplane fuselage or a space launcher undergoes, derives from various sources, and understanding the consequent perturbation propagation, is crucial to avoid catastrophic failures and lengthen its average service lifespan.

The Aerospace segment often requires light and stiff materials. This is mainly the reason why honeycomb sandwich panels are widely used there. They are well known to provide good static out of plane properties (compression) because of their high equivalent stiffness. However, the use of light cellular cores makes these structures possess a very high stiffness/mass ratio and therefore, their vibration frequency domain is usually in the high range. The solicitations mentioned before though, are in the mid-low range, and as engineered today, the periodicity possessed by sandwich panels, has not been fully exploited. Obtaining sandwich panels with improved vibroacoustic performances, at specific frequency ranges, is therefore an interesting research topic.

The response of periodic structures to external excitation has already been investigated starting from Brillouin's work [1] back in 1946. Mead et al. [2] have produced a document, summarizing almost thirty years of work carried out at the University of Southampton, demonstrating how spatial periodicity in terms of structure, material, inserts or boundary layers, interacts with travelling waves. Those periodic variations

cause some of the incident waves to be reflected and some to be transmitted. The destructive interaction, partial or full, between incident and reflected waves, causes attenuation (bandgaps) at certain frequency ranges, and therefore, periodic structures can act as passive filters. There is therefore, a relation between the geometrical dimensions of the periodic structure and the travelling wave characteristics.

Periodic structures thought, can exhibit two types of stop bands created by different phenomena: Bragg Scattering and Local Resonance. Bragg scattering stop band are consequence of the spatial periodicity just mentioned and it appears when wavelengths are on the same order as the period length. In contrary, local resonance stop bands do not necessarily require periodicity and only depend on the properties of the local resonator and therefore they can lie in the sub-wavelength regime. Each periodic structure therefore possesses bandgaps that depend upon the geometry and those are the ones we will focus on in this paper.

There are many different methods that have been developed in the years and that can be found in literature, to examine periodic structures. A good summary of those techniques which mostly are FEM derived can be found in the paper written by Hussein and Ruzzene [3].

Lately, the most commonly used one, is the Wave Finite Element Method (WFEM), where the Mass and Stiffness matrices of the single repetitive component of the periodic structure, are calculated with FEM commercial software, extracted, and used to calculate the dynamics of the structure by applying the periodicity conditions described by the Floquet-Bloch Theory. Scarpa et al. were, to the authors' knowledge, were the first ones to investigate wave propagation in a Kirigami lattice using WFEM [4].

Kirigami is an innovative way of producing cellular structures. It is an ancient Japanese form of art involving cutting and folding paper to produce tri-dimensional structures [5 - 6]. A previous work [5], attempted to produce, successfully, a cellular structure possessing zero in-plane Poisson's coefficient (AUXHEX). This was obtained using a hybrid tessellation which conferred the overall structure, the desired property. By hybrid, is intend a cellular core containing cells of different shapes. The geometrical constrain in term of final cell shape Kirigami imposes to the manufacture though, pushed the authors to develop a new technique that overcomes the limitation and allows to produce new types of hybrid tessellation. The cellular structure analysed was named HEXHEX.

In this work, numerical simulations are carried out with the aim of investigating the vibration filtering properties of this new Kirigami structure firstly using 1DWFEM and subsequently 2WFEM methods.

The aim of this work is to detect the presence of the Bragg bandgaps possessed by the HEXHEX cellular structure, and attempt to enlarge existing or open new ones, by varying its geometrical parameters. The HEXHEX hybrid core will finally be compared with two classic tessellations, Hexagonal and Re-entrant. An overview of the investigation methods as well as some considerations on the results obtained are proposed.

2 Wave propagation in periodic media

2.1 Periodic structures

A structure which exhibits some form of spatial periodicity is defined as a periodic structure. Such characteristic must be in its internal geometry, constituent material or the boundary conditions. Periodicity allows us to do some considerations about the behaviour of the full structure by carrying out analyses on just a portion of structure [4, 7-9], also known as the *unit cell*. By repeating this portion in space, we recreate the full structure (Figure 1).

2.2 Floquet-Bloch Theory

This theory is the core of the WFEM method and was firstly introduced for engineering investigations by Brillouin [1]. According to this theory, displacements and forces on the nodes on the extremities of a unit cell are related. This means that it is sufficient to analyse a small portion of our periodic structure to understand the overall dynamic behaviour.

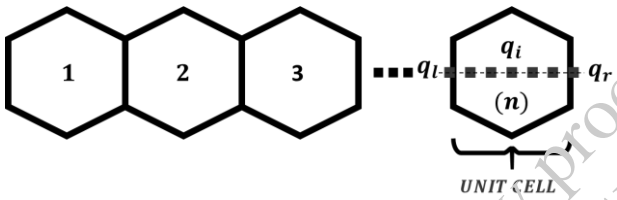

$$q_r^{(n)} = \lambda q_l^{(n)} = e^{j\mu} q_l^{(n)} \quad (1)$$

$$-f_r^{(n)} = \lambda f_l^{(n)} = e^{j\mu} f_l^{(n)} \quad (2)$$

Figure 1 - Periodic structure unit cell and 1D Floquet Bloch periodic relations

The Floquet-Bloch relations for forces (f) and displacements (q) for 1D periodicity are shown in (1) and (2) respectively, where the subscripts l and r indicate the left or right of the unit cell, $\mu = kL$ is the reduced wave number, k is the wave number and L the length of the unit cell.

To understand the dynamic behaviour of a periodic structure, a dispersion curve, which represents the relation between the reduced wavenumber (μ) versus the frequency (ω) can be plotted. To produce a dispersion curve therefore, a relation between ω and $\lambda = e^{j\mu}$ is required. The starting point is represented by the Fundamental Dynamics Equation of the unit cell. Neglecting damping, such equation becomes:

$$(K_{uc} - \omega^2 M_{uc}) \begin{pmatrix} q_l \\ q_i \\ q_r \end{pmatrix} = \begin{pmatrix} f_l \\ f_i \\ f_r \end{pmatrix} \quad (3)$$

K_{uc} and M_{uc} are the stiffness and the mass matrix respectively of the unit cell, and the objective is to convert this relation into an eigenvalue problem, by cancelling the force vector on the right-hand side.

By applying the Floquet-Bloch conditions on forces and displacements into Equation (3) the following relation that describes the dynamics of the unitcell is obtained:

$$\Lambda_L (K_{uc} - \omega^2 M_{uc}) \Lambda_R \begin{pmatrix} q_l \\ q_i \end{pmatrix} = 0 \quad (4)$$

where $\Lambda_R = \begin{bmatrix} I & 0 \\ 0 & I \\ \lambda I & 0 \end{bmatrix}$ and $\Lambda_L = \begin{bmatrix} I & 0 & \frac{1}{\lambda} I \\ 0 & I & 0 \end{bmatrix}$

The right-hand side of equation (4) is equal to zero thanks to the Floquet-Bloch relation on the forces which assumes $f_i = 0$.

$$\left(K_r(\mu) - \omega^2 M_r(\mu)\right) q^{(r)} = 0 \tag{5}$$

Finally, the standard eigenvalue problem (5) is derived and by solving for $\mu \in [0; \pi]$, which represents the First Brillouin Zone, the frequency is obtained.

This procedure is usually followed when investigating periodic structures along their direction of periodicity and therefore it is known as 1DWFEM. In the case of cellular cores though, periodicity may happen along two directions.

Wave vectors can be expressed in terms of the reciprocal lattice basis which represents the Fourier transform of a periodic spatial function in real-space also known as the direct lattice. Since the reciprocal lattice is also periodic, one can restrict the wave vectors to a certain region called first Brillouin zone.

If there is symmetry in the reciprocal lattice, the wave vectors may be further restricted to the Irreducible Brillouin Zone (IBZ) (OABC), shown in Figure 1, where the wavenumbers are positive. In some descriptions of the wave propagation characteristics, only the contour of the IBZ (O-A-B-C-O) is considered, where the band extrema almost always occur [11].

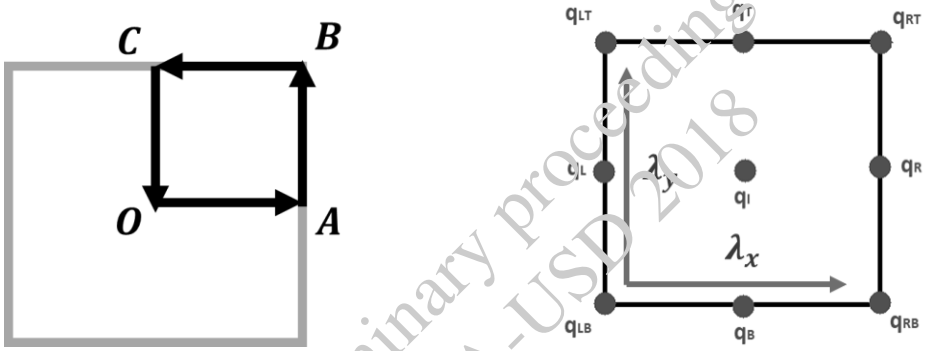

Figure 2 - Irreducible Brillouin Zone (left) and representative unit cell boundary nodes (right)

$$\begin{aligned} \lambda_x &= e^{j\mu_x} & \mu_x &= k_x L_x \\ \lambda_y &= e^{j\mu_y} & \mu_y &= k_y L_y \end{aligned} \tag{6}$$

$$\begin{aligned} q_T = \lambda_y q_B \;\; ; \;\; q_R = \lambda_x q_L \;\; ; \;\; q_{LT} = \lambda_y q_{LB} \\ q_{RB} = \lambda_x q_{LB} \;\; ; \;\; q_{RT} = \lambda_x \lambda_y q_{LB} \end{aligned} \tag{7}$$

$$\begin{aligned} f_{LB} + \lambda_x^{-1} f_{RB} + \lambda_y^{-1} f_{LT} + \lambda_x^{-1} \lambda_y^{-1} f_{RT} = 0 \\ f_L + \lambda_x^{-1} f_R = 0 \\ f_B + \lambda_y^{-1} f_T = 0 \end{aligned} \tag{8}$$

In Figure 2, a standard square 2D unit cell is represented and as the reader might have noticed, the nodes that need to be linked to analyse such periodicity are not just limited to the left and right boundaries of the cell, but also covers the bottom, top as well as the corner nodes. Equations (6) describes the 2D Floquet-Bloch relation while (7) and (8) link the cell extremities in terms of forces and displacements, just as it happened in the 1D case.

3 Hexhex pattern

Kirigami is an ancient Japanese art technique of cutting and folding paper to obtain a 3D structure. In the past [4-6] it has been used to produce cellular structures and the HEXHEX core, represents one of the many alternatives that the interlock concept is able to produce. The HEXHEX is a new interesting configuration that cannot be produced with classic Kirigami technique, due to the rhombohedral cells, but can be produced with the interlocking Kirigami derived technique.
By interlocking two hexagonal cores, we obtain the final structure which overall produces a hybrid cellular core made of different hexagonal cells as well as rhombohedral or parallelogram cells. The result of such interlocking is shown in Figure 3, where the side length of the hexagon is $l = 5\ mm$ and $t = 0.2\ mm$ the thickness of the squared cross-section beam.

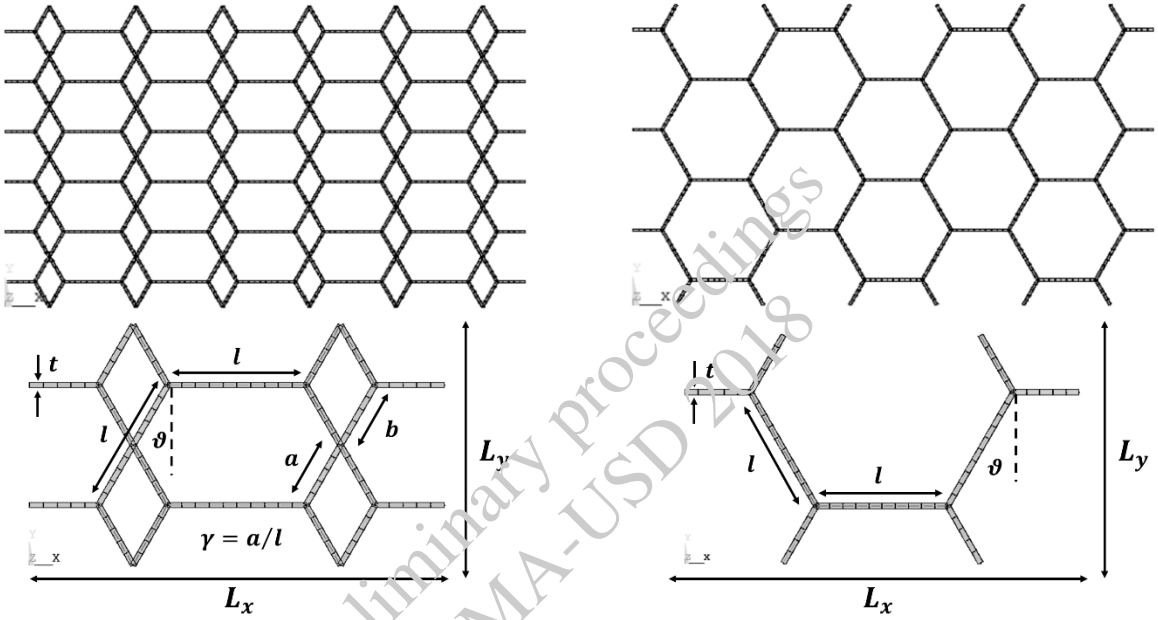

Figure 3 - HEXHEX lattice (top-left), Hexagonal lattice (top-right), HEXHEX unit cell (bottom-left), Hexagonal unit cell (bottom-right)

The investigation, both for 1D and 2D periodicity, was performed varying parameters like the shift ratio (which happens in the Y direction) between the two hexagonal cores $\gamma = a/l$, where $l = a + b$, and then the hexagonal internal angle ϑ. As shown in Figure 4, when the shift ratio is varied, the unit cell overall dimensions L_x and L_y are kept constant. This also means, since the core thickness in the Z direction is constant, that the overall relative density of the core will be constant and therefore the compression static properties in the Z direction will be equal [10].

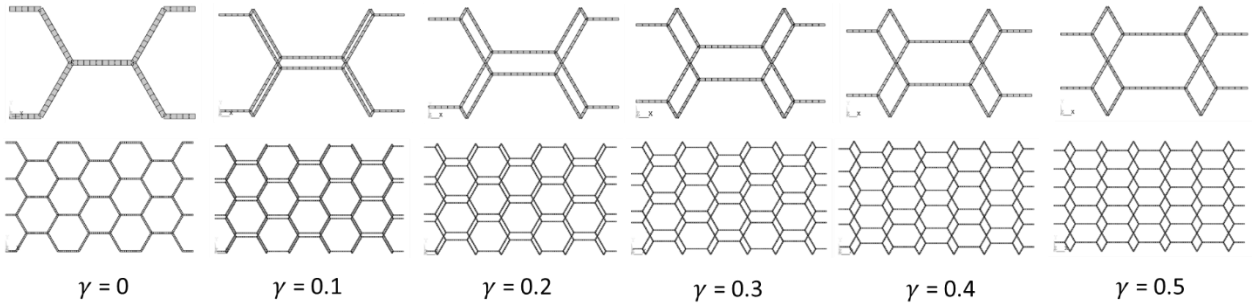

Figure 4 - HEXHEX unitcells (top) and respective representative lattices (bottom) for variable shift ratio

4 Investigation methods

As mentioned in the introduction, the objective is to perform vibration analyses on the HEXHEX topology to see whether it possesses in plane and/or out of plane Bragg bandgaps. The parameter taken into consideration to evaluate the topology performance is the presence and width of bandgaps.

Before proceeding with the actual bandgap evaluation, agreement between the bandgaps found using commercial software to produce FRF's and the ones found using Wave Finite Element Method (WFEM) will be carried out for the Hexagonal configuration, which has been chosen as the reference.

For the analysis, Timoshenko beam elements have been used as in this way, uncoupling of in-plane and out-of-plane behavior was possible. The element size for all the numerical simulations was set to 0.5mm and the material properties as well as variable parameters are listed in Table 1.

$\boldsymbol{Young's\ Modulus, E\ [GPa]}$	8.1
$\boldsymbol{Density, \rho\ [kg\ m^{-3}]}$	1040
$\boldsymbol{Poisson's\ Ratio, \upsilon}$	0.2
$\boldsymbol{Shift\ Ratio, \gamma}$	[0 - 1]
$\boldsymbol{Internal\ angle, \vartheta}$	[10° - 85°]

Table 1 - Numerical simulation parametric analysis variables and material properties

The Frequency response plot, obtained with a Harmonic simulation of the finite structure, is used to illustrate the validity of the bandgaps locations, as the amplitude drop of the plot increases with the increase of the number of unit cell repetitions.

The Harmonic analysis consisted in applying a compression force at one end of a truss structure created with repetition of unit cells along the periodicity direction. The out-of-plane degrees of freedom were blocked. The displacement amplitude of the selected nodes at the extremities of the truss was extracted and used to plot the FRF. The same type of harmonic study was carried out applying a bending (in-plane) force and recording displacements in the Y direction.

The 1D periodicity was analysed using the direct WFEM, which makes use of the Floquet Bloch theory to produce dispersion curves linking frequency (input) with the reduced wave number. For the 2D periodicity dynamic analysis, instead, the inverse WFEM form was used. In this method, the reduced wavenumber is imposed, and the output frequency calculated. In-plane and out-of-plane analysis was carried out.

4.1 Method validation (Hexagonal 1D)

The unit cell as well as a representation of the hexagonal topology are shown in Figure 5

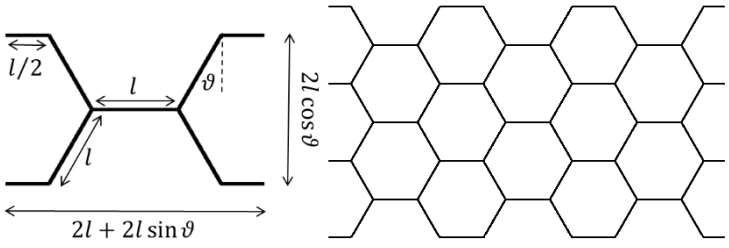

Figure 5 - Hexagonal unit cell and representative lattice

Figure 6 shows the FRF plots and the dispersion curves for the hexagonal topology. The graphs present vertical grey bands in correspondence of the bandgaps for clearness purposes. There is very good correspondence between dispersion curves (infinite structure) and the computed FRF plots (finite structure) and therefore from now on, we will only produce dispersion curves, as with a single simulation, we are able to identify the bandgaps without having to perform two different simulations.

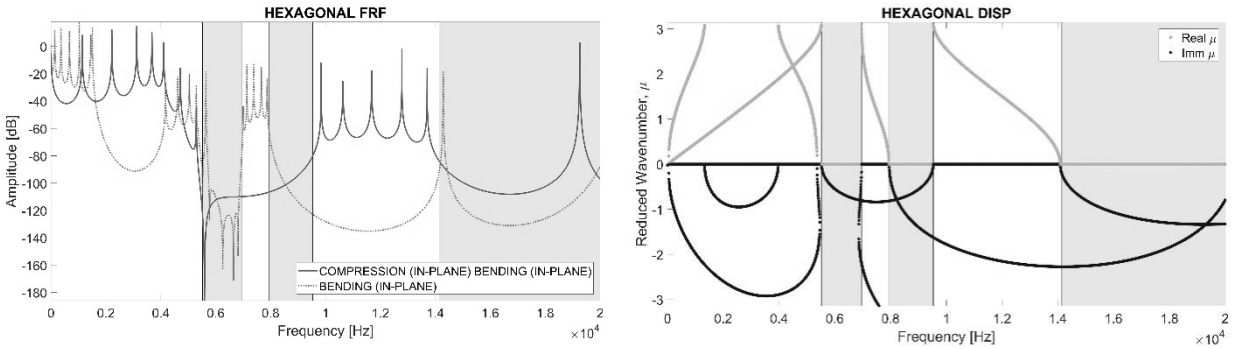

Figure 6 - Hexagonal lattice FRF (left) and Dispersion curves (right)

Since no damping was considered in the model, the amplitude scale of the FRF graph (Figure 6 left) loses its meaning. The intention here is just to use these plots as a visual tool to identify the frequency range of the bandgaps.

4.2 1DWFEM (in-plane)

Figure 7 shows the unit cells used for this type of analysis. In Figure 8 instead, two extreme configurations (for $\gamma = 0$ and $\gamma = 1$) representing regular hexagonal lattices are shown. To keep static out of plane properties constant, walls for those configurations were doubled where appropriate.

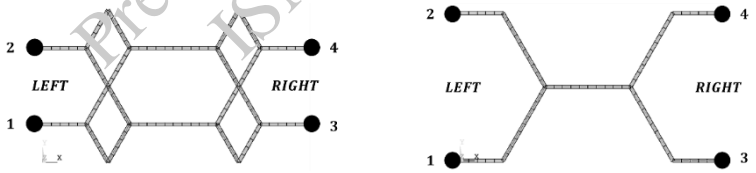

Figure 7 - 1DWFEM unitcells for HEXHEX (left) and HEXAGONAL (right) configurations

4.2.1 Variable shift ratio

The analysis will be carried out keeping $\vartheta = 30°$ and $l = 5mm$ constant. As consequence, a constant relative density is obtained since L_x and L_y do not vary, as shown in Figure 8. The shift only happens in the Y direction.

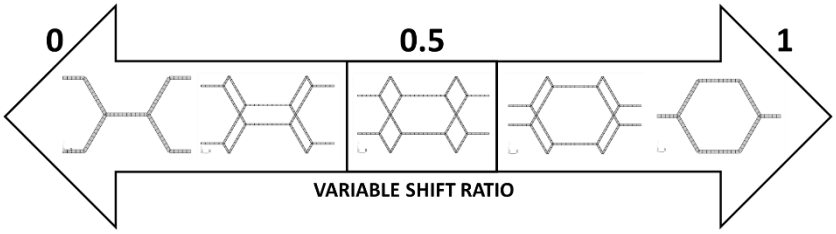

Figure 8 – HEXHEX unit cells according to the shift ratio variation

In Figure 9 (left) the dispersion plot for all the configurations are shown. Apparently, a minimum shift between the two initial hexagonal cores produces a bandgap that begins at 7410 Hz and has a bandwidth of 8910 Hz (see shift ratio $\gamma = 0.1$). For the latter shift ratio, we also obtain three very narrow bandgaps respectively starting at 4120 Hz, 17980 Hz and finally 18370 Hz. It is interesting also to point out how for $\gamma = 0$ and $\gamma = 1$ we obtain the same dispersion curves as their respective unit cell is the same one but simply shifted. Both unit cells maintain X and Y-axis symmetry and are therefore defined as being centrosymmetric.

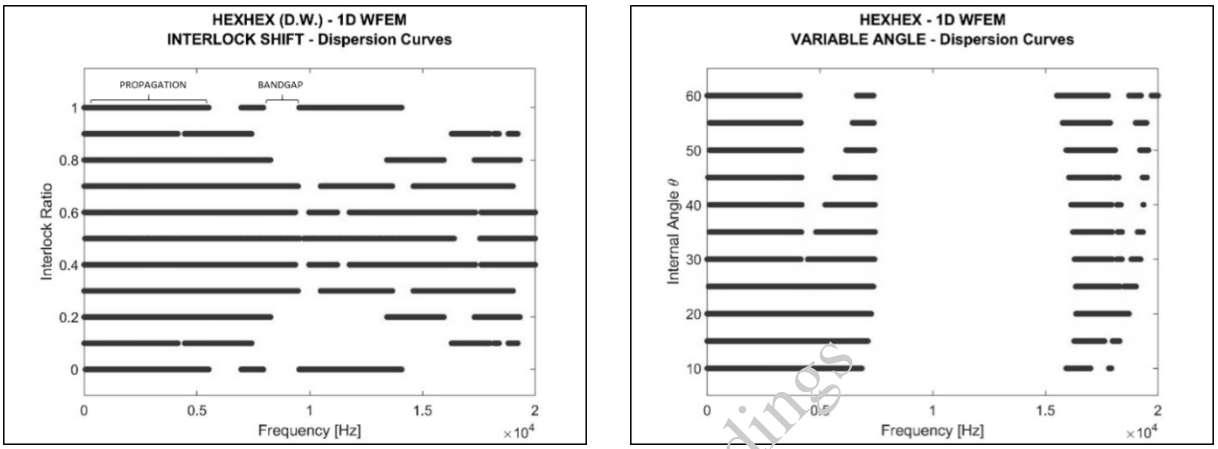

Figure 9 - 1DWFEM Dispersion curves for variable shift ratio (left) and variable internal angle with fixed shit ratio (right)

4.2.2 Variable internal angle

The variable angle analysis will be carried out keeping γ and l constant and the direct consequence is the change of relative density since L_x and L_y vary, as shown in Figure 10. The selected configuration to perform a variable angle analysis was the $\gamma = 0.1$ as it possessed the wider bandgap (8910 Hz) at lower frequencies (both aspects are within the investigation aim).

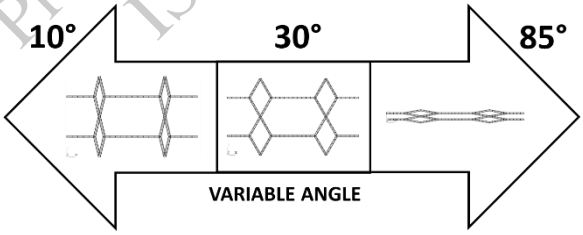

Figure 10 - HEXHEX unit cells according to internal angle variation

In Figure 9 (right) the dispersion plots for all the variable angle configurations are shown. The variation of the internal angle ϑ has a minimum effect upon the large bandgap which we observed during the shift ratio analysis (its width drops to 8170 Hz), but it opens up two of the minor bandgaps. The one starting at 4120 Hz, enlarges, keeping its left boundary roughly fixed and changing from an initial width of only 345 Hz to a width of 2580 Hz. The bandgap appearing at 17980 Hz tends to close as we increase ϑ, but the bandgap starting at 18370 Hz and finishing at 18830 Hz (width of 460 Hz) maintains the right boundary fixed and enlarges the left one reaching a width of 950 Hz.

4.3 2DWFEM

The unitcells used for the bidimensional periodicity analysis of the two cores are shown in Figure 11. We will perform both in-plane as well as out-of-plane analyses this time, contrary to the 1D periodicity case.

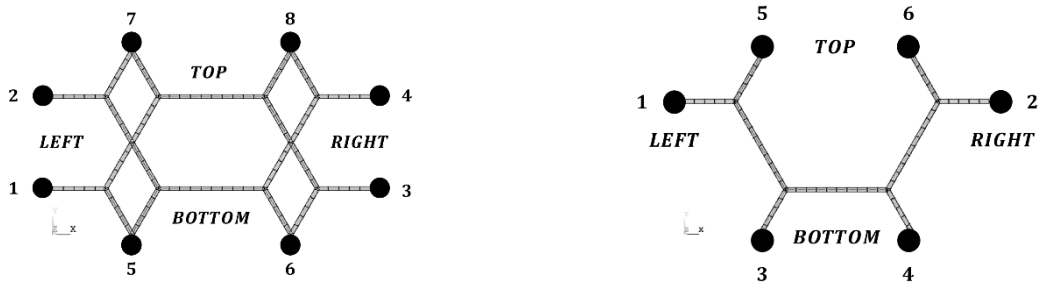

Figure 11 - 2DWFEM unitcells for HEXHEX (left) and HEXAGONAL (right) configurations

4.3.1 Hexagonal 2D

Figure 12 (top-left and top-right) shows respectively the 2D dispersion relation of a regular hexagonal lattice with $\vartheta = 30°$ and $l = 5mm$. Both in-plane and out-of-plane hexagonal configurations do not show presence of full bandgaps.

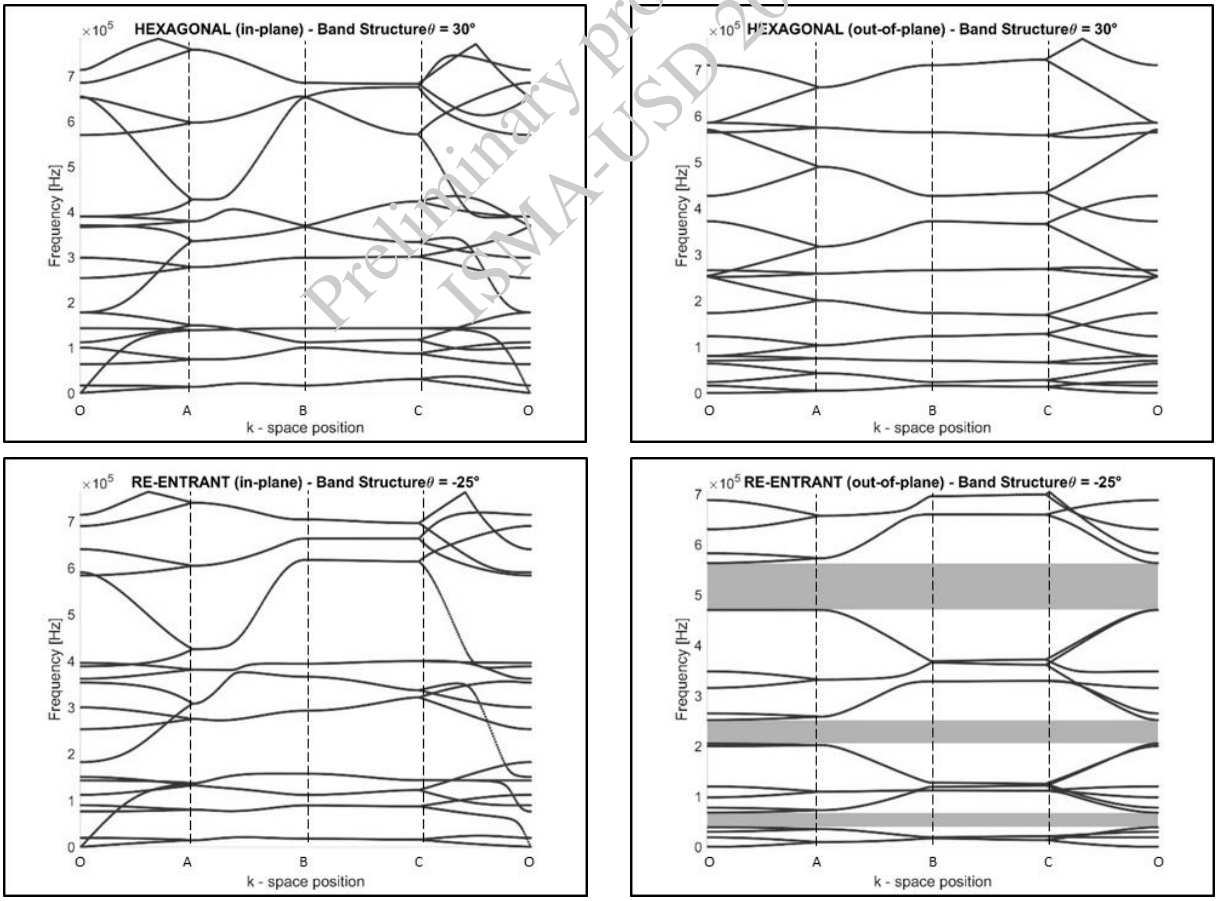

Figure 12 - 2DWFEM dispersion curves for Hexagonal/Re-entrant configuration (In-plane and out-of-plane)

When we vary the internal angle though shifting from a hexagonal to a re-entrant lattice, bandgaps in the out-of-plane analysis appear, as shown in Figure 12 (bottom-right). The respective bandgap widths starting from lower frequencies are: 29.12 kHz, 46.70 kHz and 92.90 kHz.

4.3.2 Hexhex

Figure 13 shows respectively the 2D dispersion relation in-plane and out-of-plane for the initial HEXHEX lattice with $\vartheta = 30°$, $\gamma = 0.5$ and $l = 5mm$. The in-plane configuration does not show presence of full bandgaps, just like the hexagonal case. The out-of-plane configuration instead does, and its bandwidth is 6.70 kHz.

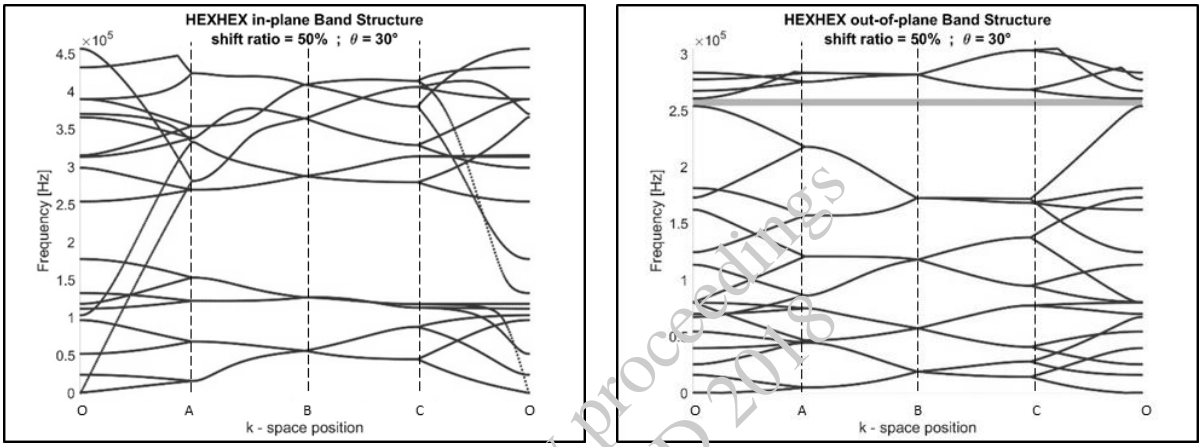

Figure 13 - 2DWFEM HEXHEX initial configuration dispersion curves (γ= 0.5; ϑ = 30°) in-plane and out-of-plane

Keeping in mind the initial objective, we varied ϑ and γ within the range listed in Table 1 and we obtained the following results, listed in Table 2 and Table 3. The variation of those parameters creates, and in some cases enlarges pre-existing bandgaps.

Figure 14 shows the configurations which exhibited the larger bandgaps. The widest in-plane full bandgap was obtained for $\vartheta = 35°$, $\gamma = 0.2$ (Figure 14 left) with a value of 9.90 kHz, whilst out of plane, for $\vartheta = 65°$ and $\gamma = 0.5$ (Figure 14 right) with a value of 16.40 kHz.

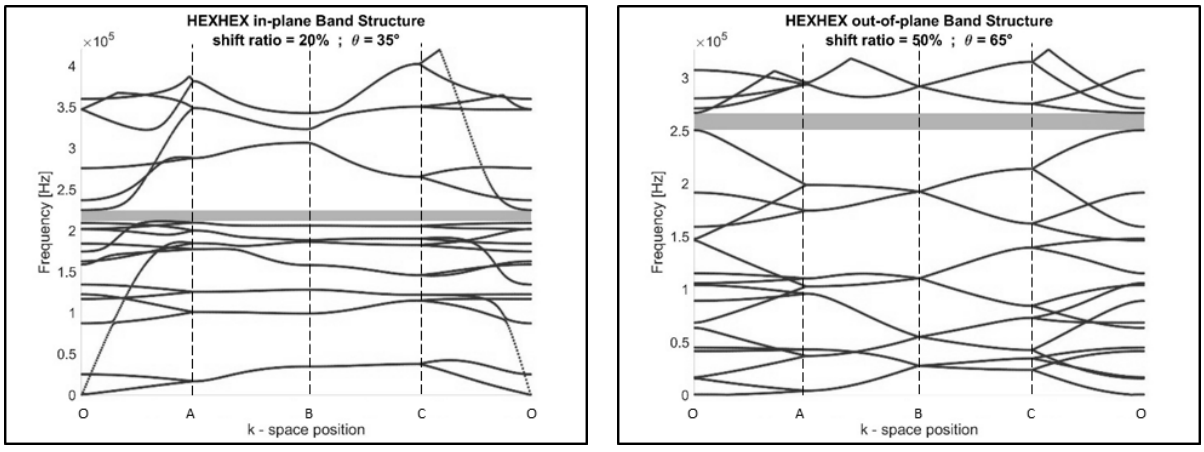

Figure 14 - 2DWFEM HEXHEX dispersion curves. In-plane and out-of-plane best performance obtained

It is worth to show (Figure 15) that for a combination of $\vartheta = 70°$ and $\gamma = 0.3$, there are 3 bandgaps, just like we obtain for the re-entrant configuration, although their width is considerably smaller if compared to those ones. The values from lower frequencies to higher ones are 5.40 kHz, 2.30 kHz and 7.60 kHz

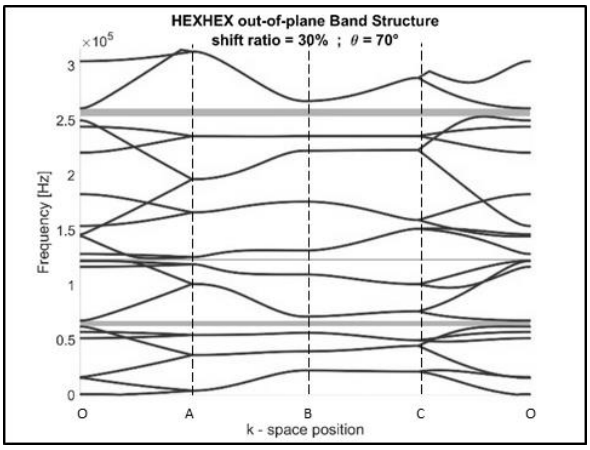

Figure 15 - 2DWFEM HEXHEX configuration (γ= 0.5; ϑ = 30°) with the highest number of bandgaps

5 Conclusions

The implementation of the Floquet-Bloch periodic boundary conditions through a transfer matrix method for 1D vibration bandgap prediction as well as for 2D periodicity is a valuable investigation resource, since the numerical results obtained agree with the ones obtained using commercial software.

The 1DWFEM analysis (Figure 9) shows that the HEXHEX lattice possesses bandgaps just like periodic mediums are supposed to do, and that the selected variables shift ratio (γ), and internal angle (ϑ), affect both the appearing of bandgaps as well as changing its width. In particular, for variable γ, the widest bandgap was produced when $\gamma = 0.1$ and $\vartheta = 30°$ was kept fixed. By selecting the latter configuration to vary ϑ this time, we observed that when $\vartheta = 60°$ the main bandgap keeps its width roughly constant the bandgap around 4500 Hz which is initially only 345 Hz wide, enlarges up to 2580 Hz as well as the one starting at 18370 Hz and finishing at 18830 Hz (width of 460 Hz) which reaches a width of 950 Hz.

The configuration that meets our goal for the 1DWFEM study is therefore $\gamma = 0.1$ and $\vartheta = 60°$.

The 2DWFEM analysis reveals that the regular hexagonal lattice does not possess full bandgaps both in-plane and out-of-plane. By varying the internal angle and reaching therefore the re-entrant configuration ($\vartheta = -25°$), three bandgaps appear with widths, starting from lower frequencies, of 29.12 kHz, 46.70 kHz and 92.90 kHz respectively.

The HEXHEX 2DWFEM analysis shows that this lattice is able to produce both in-plane and out-of-plane bandgaps. Figure 14 shows the configurations which exhibited the larger bandgaps. The widest in-plane full bandgap was obtained for $\vartheta = 35°$, $\gamma = 0.2$ (Figure 14 left) with a value of 9.90 kHz, whilst out of plane, for $\vartheta = 65°$ and $\gamma = 0.5$ (Figure 14 right) with a value of 16.40 kHz.

Although the largest bandgap recorded was obtained with the re-entrant configuration, the HEXHEX lattice represents a valid competitor for the classic hexagonal lattice.

6 Acknowledgements

I would like to express all my gratitude to [1]Université Bourgogne Franche Comté and [2]University of Bristol for hosting me during my research, and to my supervisor Morvan Ouisse[1] and Fabrizio Scarpa[2]. I would also like to thank my VIPER MSCA-ITN colleagues for constant feedback.

This project has received funding from the European Union's Horizon 2020 research and innovation programme under Marie Curie grant agreement No 675441 and was performed in collaboration with EUR EiPHi Project (ANR 17-EURE-0002).

7 References

[1] L. Brillouin. Wave propagation in periodic structures, electric filters and crystal lattices. Dover, 1953.
[2] D.J. Mead. Wave propagation in continuous periodic structures: research contributions from southampton 1964-1995. J. Sound Vib., 190(3):495-524, 1996.
[3] M I Hussein, M J Leamy, and M Ruzzene. Dynamics of phononic materials and structures: Historical origins, recent progress and future outlook. Applied Mechanics Reviews, 66(4):040802, 2014.
[4] F. Scarpa, M. Ouisse, M. Collet, K. Saito Kirigami Auxetic Pyramidal Core: Mechanical Properties and Wave Propagation Analysis in Damped Lattice. ASME. J. Vib. Acoust. 2013;135(4):041001-041001-11. doi:10.1115/1.4024433.
[5] S. Del Broccolo, S. Laurenzi, & F. Scarpa, 2017, 'AUXHEX – a Kirigami inspired zero Poisson's ratio cellular structure'. Composite Structures, vol 176., pp. 433-441.
[6] Neville, R.M., et al., Transverse stiffness and strength of Kirigami zero-ν PEEK honeycombs. Composite Structures, 2014. 114: p. 30-40.
[7] F. Scarpa, M. Ruzzene - Wave beaming effects in two-dimensional cellular structures, Smart Materials and Structures, 12 (2003) 363 – 372.
[8] Brian R. Mace, Denis Duhamel, Michael J. Brennan - Finite element prediction of wave motion in structural waveguides, The Journal of the Acoustical Society of America – 117 (2005) 2835-2843.
[9] Brian R. Mace, E. Manconi - Modelling wave propagation in two-dimensional structure using finite element analysis, Journal of Sound and Vib. 318 (2008) 844 – 902.
[10] Lorna J, Gibson MFA. Cellular Solids. 2nd Ed. Cambridge University Press, 1997.
[11] Kittel C. Introduction to Solid State Physics. Wiley, 8th edition. 11, 43.

8 Appendix

	HEXAGONAL $\vartheta \geq 0$		**HEXHEX** $\vartheta \geq 0$									
	In-plane	Out-of-plane	In-plane					Out-of-plane				
ϑ \ γ	0 & 1		0.1	0.2	0.3	0.4	0.5	0.1	0.2	0.3	0.4	0.5
10	0	2	0	0	0	0	0	0	0	0	0	1
15	0	1	0	0	0	0	0	0	0	1	0	1
20	0	0	0	0	0	0	0	0	0	1	0	1
25	0	0	0	0	0	0	0	0	0	1	1	1
30	0	0	0	1	1	0	0	0	0	0	1	1
35	0	0	0	1	1	0	0	0	0	0	0	1
40	0	0	0	1	1	0	0	0	0	0	0	0
45	0	0	0	1	0	0	0	0	0	0	0	0
50	0	1	0	0	0	0	0	0	1	0	0	0
55	0	1	0	0	0	0	0	0	1	0	0	1
60	0	1	0	0	0	0	0	1	0	0	0	1
65	0	1	0	0	1	0	0	1	0	2	1	1
70	0	1	1	0	1	0	0	1	0	3*	1	1
75	0	1	0	0	1	0	0	1	0	3*	1	1
80	0	1	0	0	0	0	0	1	0	2	1	1
85	0	1	0	0	0	0	0	1	0	1	0	0
* = Maximum number of bandgaps ; ___ = Maximum bandgap width reached												

Table 2 - 2DWFEM simulation summary

	HEXAGONAL $\vartheta \leq 0$ (Re-entrant configuration)									
	In-plane					Out-of-plane				
γ \ ϑ	-25	-20	-15	-10	0	-25	-20	-15	-10	-0
0 & 1	0	0	0	0	0	3 *	3*	3*	3*	3*
* = Maximum number of bandgaps ; ___ = Maximum bandgap width reached										
The HEXHEX configuration with this unit cell could not be used for $\vartheta \leq 0$										

Table 3 - 2DWFEM simulation summary bis

8.1 List of tables

8.2 List of figures